J. Fluid Mech. (1977), *vol.* 82, *part* 1, *pp.* 179–191
Printed in Great Britain

On choking flutter

By Y. TANIDA AND Y. SAITO†
Institute of Space and Aeronautical Science, University of Tokyo, Japan

(Received 18 October 1976)

The purpose of the present study is to assess the possibility of the so-called choking flutter in a transonic cascade operating under choking conditions. In the experiment, measurements of the unsteady aerodynamic moment acting on an aerofoil which is oscillating in pitch about the midchord in a transonic channel flow are performed for channel height-to-chord ratios $H/c = 0{\cdot}5$–3 and oscillation frequencies up to 120 Hz. For a large channel height such as $H/c = 3$, the unsteady aerodynamic behaviour is similar to that of an isolated aerofoil, and the system will be aeroelastically stable in the transonic region as well as in the subsonic one. For smaller channel heights such as $H/c = 0{\cdot}5$, however, the flow chokes and the aerodynamic behaviour becomes significantly different from that at large channel heights. As soon as a shock appears, i.e. in the incipient transonic region, the aerodynamic derivatives change discontinuously, so that the subsonic and transonic regions can be clearly separated. In this case, the aerodynamic damping becomes negative in the transonic region.

In order to understand the transonic features, a one-dimensional unsteady analysis is undertaken for small channel heights $H/c \leqslant 0{\cdot}5$. The numerical results show good qualitative agreement with the experimental ones, predicting in the incipient transonic region a discontinuous variation of the aerodynamic moment which results in system instability.

It is concluded that choking flutter may occur in transonic channel flow with a moderately small channel height when the passage is choked.

1. Introduction

During the past two decades the advent of the lightweight high-speed advanced aeroengine has stimulated interest in the flutter problem of aerofoils in cascades. The classical flutter problem in incompressible and subsonic compressible flows has been exhaustively discussed. The current interest is mainly directed towards elucidating the aeroelastic characteristics of an unstalled supersonic cascade with a subsonic leading edge.

Choking flutter is another type of flutter which may occur in a cascade; the cascade may be choked owing to the blocking action of the blade thickness when the inlet flow is either high subsonic or low supersonic. In this state the aeroelastic instability of the blades may be significantly affected both by choking and by the appearance of shocks which move with the vibration of the blades. This so-called choking flutter is less common than the other types of flutter, so that only a few references to it have appeared in the literature (Carter & Kilpatrick 1957; Mikolajczak *et al.* 1975).

† Present address: National Aerospace Laboratory, Chofu, Tokyo, Japan.

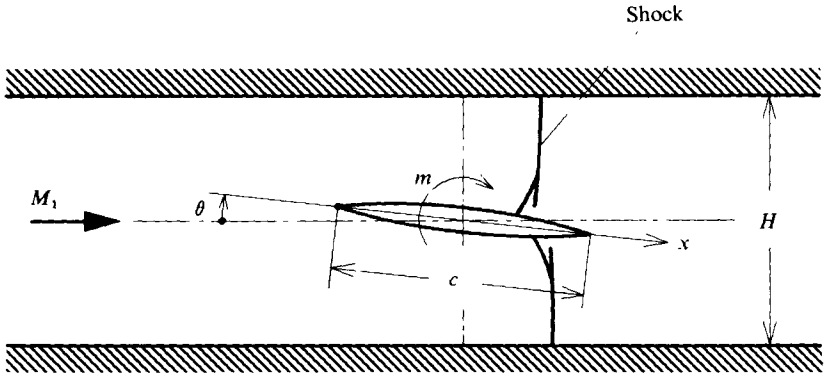

FIGURE 1. Schematic diagram of system investigated.

Choking flutter is also likely to arise in high-speed ground transport systems in which vehicles travel through tubes. Several studies have been made of the aerodynamics of vehicles travelling either in tubes or in tunnels and showed that transient motions can occur during acceleration or deceleration or when the tunnel has a finite length (Hammitt 1975). At moderate subsonic vehicle speeds the flow will be accelerated through the narrow annular passages about the vehicle to reach a state of Mach number unity, indicating that attention should be paid to the aeroelasticity in such tube vehicle systems as well as in turbomachines.

The purpose of the present study is to assess the possibility of choking flutter, first through a fundamental experiment and then through a one-dimensional theoretical approach. The system considered will be the simplified two-dimensional system shown in figure 1, in which a single oscillating aerofoil with a subsonic leading edge is located on the channel axis between parallel walls.

2. Description of experiment

The blowdown test facility used in the present study consists of an air supply tank, a settling chamber, a rectangular test section and an exhaust surge tank. By means of an automatic valve-control system, filtered dry air is supplied from the supply tank to the settling chamber, which essentially acts as a stagnation plenum with normal temperature. Figure 2 (plate 1) shows the test section (one of the side walls being removed) and the aerofoil oscillation system. The model is installed in the test section, which is 75 mm wide by 200 mm (maximum) high, between two parallel end walls. The vertical position of each end wall is adjustable to allow the various wall effects on the model to be studied, but in the present study they were always positioned such that the model was situated on the channel axis.

The model used in this experiment is a symmetrical double-circular-arc aerofoil of 10 % thickness with a chord of 50 mm and fully spans the distance between the side walls of the wind tunnel. The aerofoil is cantilevered and oscillated in pitch about the midchord by the oscillation mechanism. Two electromagnetic shakers drive cross-arms to oscillate a torsion rod which is connected to the aerofoil by a ring balance. The torsion rod is used as an amplitude amplifier for angular displacement of the aerofoil. Strain

gauges are mounted on the spring bearing and ring balance to detect the torsional displacement and aerodynamic moment of the aerofoil respectively.

In oscillation tests, the signals from the strain gauges are recorded on an FM tape recorder, being reproduced after the tests on a pen plotter. By eliminating the inertial effects of real and apparent mass from the overall signals, the vector representing the fundamental component of the aerodynamic moment can be plotted against the angular displacement. The chordwise steady pressure distribution about the aerofoil is measured separately by using another model with ten pressure tappings.

A double-pass schlieren system is used for flow visualization. One of the wind-tunnel side walls, through which the aerofoil axis passes, is backed by a glass mirror to serve as a reflective surface for the beam.

The principal conditions of the tests may be summarized as follows. Four channel heights were chosen: $H/c = 0{\cdot}5$, 1, 2 and 3. The inlet flow was subsonic with a Mach number exceeding 0·5, while the Reynolds number ranged from $0{\cdot}63 \times 10^6$ to $1{\cdot}16 \times 10^6$. The mean and oscillatory angles of attack were 0 and 0·5° respectively. The maximum oscillation frequency in the tests was $f = 120$ Hz. If a non-dimensional frequency parameter (or reduced frequency) is defined as $k = 2\pi fc/a_0$, where a_0 is the velocity of sound at the stagnation temperature, the maximum frequency corresponds to $k = 0{\cdot}110$.

The flow conditions of the tests were controlled by varying the back-pressure ratio p_2/p_0, where p_2 and p_0 are the back pressure and inlet stagnation pressure respectively. As the back-pressure ratio is lowered below a critical value, the passages around the aerofoil become choked and the inlet Mach number reaches a limit when the flow upstream of the shock becomes independent of the back-pressure ratio. At smaller channel height-to-chord ratios the critical back-pressure ratio is larger and the critical inlet Mach number lower. The data here will be given in terms of the back-pressure ratio p_2/p_0 rather than the inlet Mach number since the latter does not necessarily characterize an internal transonic flow so well. The term *transonic* implies here that the flow may contain both subsonic and supersonic regions, with accompanying shocks and/or choking. The range of the back-pressure ratio extends from pure subsonic states to a limiting transonic state where the shocks reach the trailing edge.

3. Experimental results

As is well known for an isolated aerofoil, the aerodynamic derivatives of an oscillating aerofoil are highly complex in the transonic regime. The discontinuous variation of aerodynamic vectors with a slight change in Mach number may be ascribed to the appearance of shocks which fluctuate considerably both in position and in strength. The high-speed schlieren movies showed that the shocks oscillated with somewhat random unsteady motion. This random nature of the shocks was discernible when they were weak, and near the geometrical throat. As a result, the aerodynamic derivatives of an oscillating aerofoil vary from cycle to cycle, so that the data must usually be averaged over a number of cycles. This random nature, however, is expected to have a close relationship with fluctuations in the back-pressure ratio, which are inevitable in a real transonic flow. Hence, in the present study an individual value of an aerodynamic vector representing the fundamental component is obtained every ten cycles over a time history of at least one-hundred cycles in each test run.

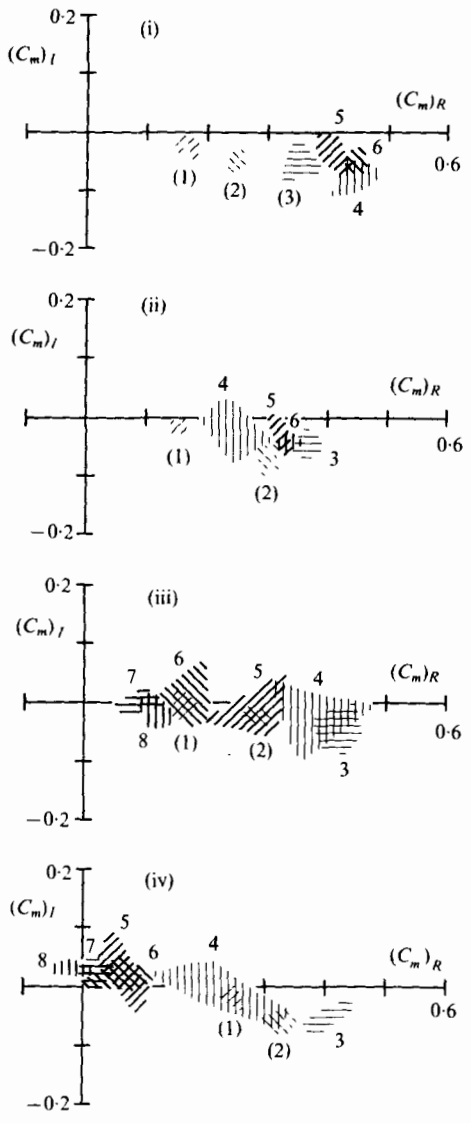

FIGURE 3(*a*). For legend see next page.

The coefficient of the fundamental component $\overline{m}\exp i\omega t$ of the aerodynamic moment per unit span for a pitching oscillation $\overline{\theta}\exp i\omega t$ is defined as

$$C_m = \overline{m}/p_0 c^2 \overline{\theta} = (C_m)_R + i(C_m)_I.$$

The vibration of the aerofoil becomes aerodynamically unstable when the imaginary part of the complex moment coefficient is positive.

Measurements of the complex aerodynamic moment coefficient for several channel heights are presented as functions of the back-pressure ratio p_2/p_0 in figures 3(*a*) and (*b*) for reduced frequencies $k = 0{\cdot}055$ and $0{\cdot}092$ respectively. The shaded regions

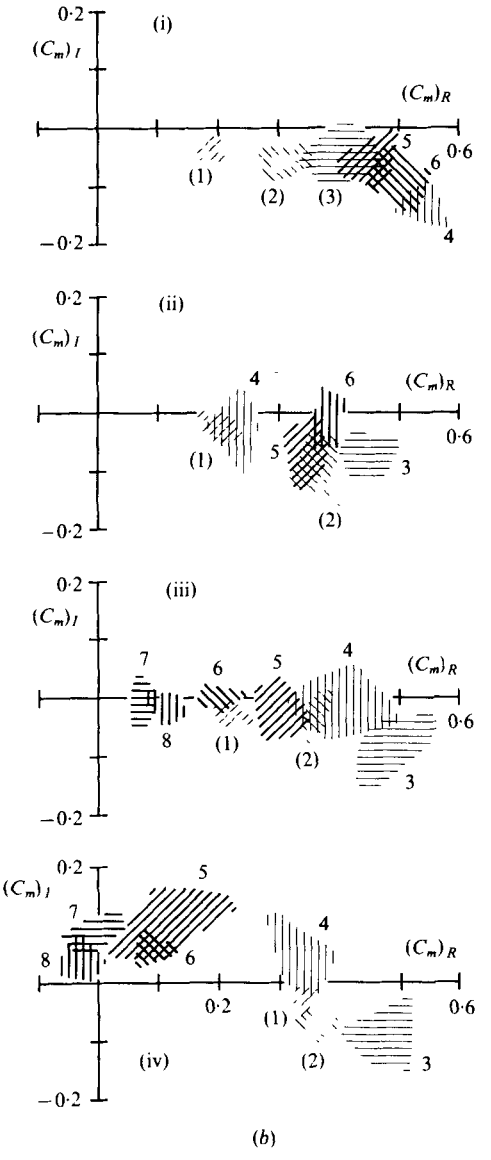

(*b*)

FIGURE 3. Moment coefficient due to pitching oscillations. (*a*) $k = 0{\cdot}055$. (*b*) $k = 0{\cdot}092$.

(i) $H/c = 3$		(ii) $H/c = 2$		(iii) $H/c = 1$		(iv) $H/c = 0{\cdot}5$	
	p_2/p_0		p_2/p_0		p_2/p_0		p_2/p_0
(1)	0·839	(1)	0·833	(1)	0·833	(1)	0·800
(2)	0·712	(2)	0·712	(2)	0·718	(2)	0·750
(3)	0·648	3	0·656	3	0·655	3	0·710
4	0·606	4	0·615	4	0·633	4	0·676
5	0·594	5	0·593	5	0·616	5	0·642
6	0·590	6	0·589	6	0·586	6	0·610
				7	0·580	7	0·594
				8	0·579	8	0·577

represent the ranges of the data obtained at the various back-pressure ratios and are numbered in order of decreasing back-pressure ratio. A number in parentheses indicates a subsonic region, e.g. region (1) corresponds to the inlet Mach number $M_1 \simeq 0{\cdot}5$, while a number not in parentheses indicates a transonic region, e.g. region 8 corresponds to the limiting transonic state in which the shocks reach the trailing edge. It should be noted that marked variations in the moment characteristics can be seen for the different channel heights, but not for the two frequencies considered.

For a large channel height such as $H/c = 3$, the unsteady aerodynamic characteristics are similar to those for an isolated aerofoil. As the back-pressure ratio is reduced (i.e. as the inlet Mach number increases), the magnitude of the complex moment coefficient increases monotonically in the subsonic region and tends to fluctuate in the transonic region, while the phase angle undergoes only a slight change and is always negative. Hence the system should be stable in the transonic region as well as in the subsonic region, although the scatter of the data appears to be rather marked in the transonic state.

For a small channel height, however, the unsteady aerodynamic characteristics become significantly different from those for a large channel height. For $H/c = 0{\cdot}5$, for example, it is evident from figures 3 (*a*, iv) and (*b*, iv) that the subsonic and transonic regions are distinctly separated, with a discontinuous change in the incipient transonic region. As soon as shocks appear, extending over most of the stream, i.e. in the incipient transonic region, a slight reduction of the back-pressure ratio causes not only a marked decrease in the magnitude of the complex aerodynamic moment but also an advance of the phase angle, which then leads the angular displacement, resulting in system instability. Deep in the transonic region the aerodynamic moment coefficient fluctuates and is likely to tend towards a limiting value as the shocks move rearwards. Scatter of the data is particularly marked in the incipient transonic region, but it should be noted that the scatter very likely follows the back-pressure variation during the tests.

Analyses of high-speed schlieren photographs of the time-dependent phenomena were also made, but have not so far been successful in finding a clear relation between the shock motion and the aerodynamic characteristics of the oscillating aerofoil. Nevertheless, the above-mentioned results may sufficiently emphasize the significance of the unsteady shock behaviour for the aeroelastic characteristics of an aerofoil oscillating in transonic channel flow, especially when the passage is choked.

4. Theoretical approach

Description of model

To approach an understanding of the unusual features of an oscillating aerofoil in a transonic channel flow described above, a one-dimensional unsteady analysis is undertaken for a case similar to the experiment. The flow model is shown in figure 4. Application of one-dimensional theory to the present problem would seem appropriate for small channel heights $H/c \leqslant 0{\cdot}5$.

The governing differential equations for one-dimensional unsteady flow are given in the appendix. By using a finite-difference method, numerical calculations have been carried out. The assumptions made in this analysis are as follows.

(*a*) One-dimensional adiabatic flow of a perfect gas is assumed. For any fluid mass, the entropy is maintained constant except at the shock.

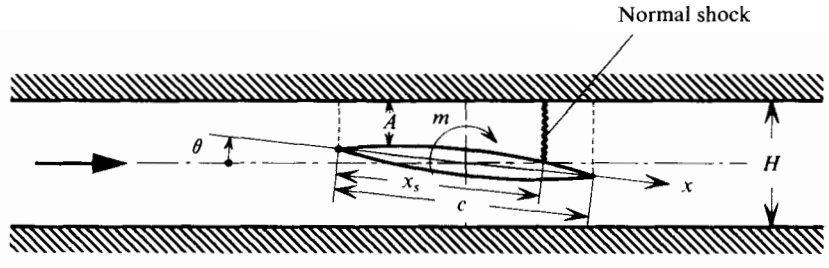

FIGURE 4. Theoretical model and notation.

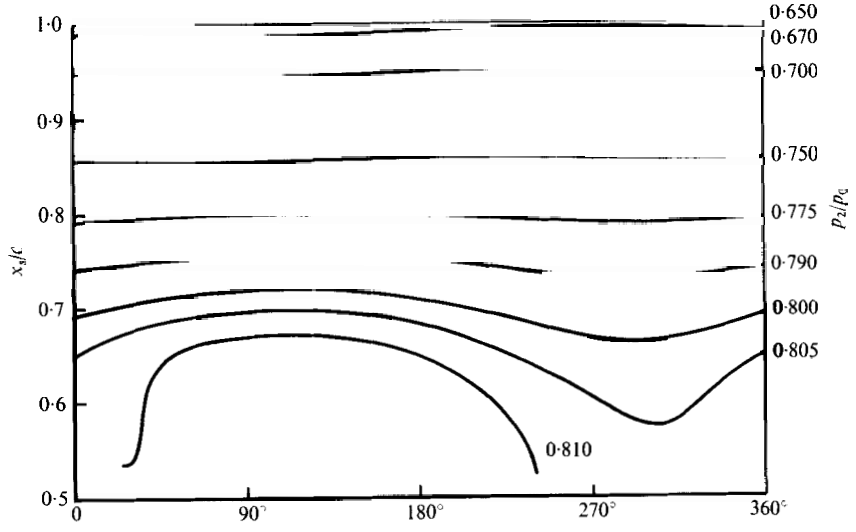

(*b*) The oncoming flow is subsonic and normal shocks are assumed to occur when the aerofoil passages are choked. The inlet conditions are fixed values of the stagnation temperature and entropy at the leading edge, while the exit condition is constant static pressure at the trailing edge.

(*c*) A similar geometry to that used in the experiments is assumed: a symmetrical double-circular-arc aerofoil of 10 % thickness is placed at zero mean incidence on the channel axis and oscillates in pitch about the midchord with a small angular displacement.

Results and comparison with experiment

Figures 5 and 6 present the calculated results for $H/c = 0{\cdot}5$, $\bar{\theta} = 0{\cdot}5°$ and $k = 0{\cdot}092$. Figure 5 shows the time history of the shock locations on the upper surface of the oscillating aerofoil as a function of the back-pressure ratio p_2/p_0. It may be seen from this figure that, in the incipient transonic region, where the back-pressure ratio is relatively large, the unsteady weak shock travels fore and aft extensively in a non-sinusoidal manner, vanishing occasionally. As the shock drifts rearwards with decreased back-pressure ratio, the displacement of the shock is much reduced and tends to a sinusoidal variation. Figure 6 presents the calculated time history of the

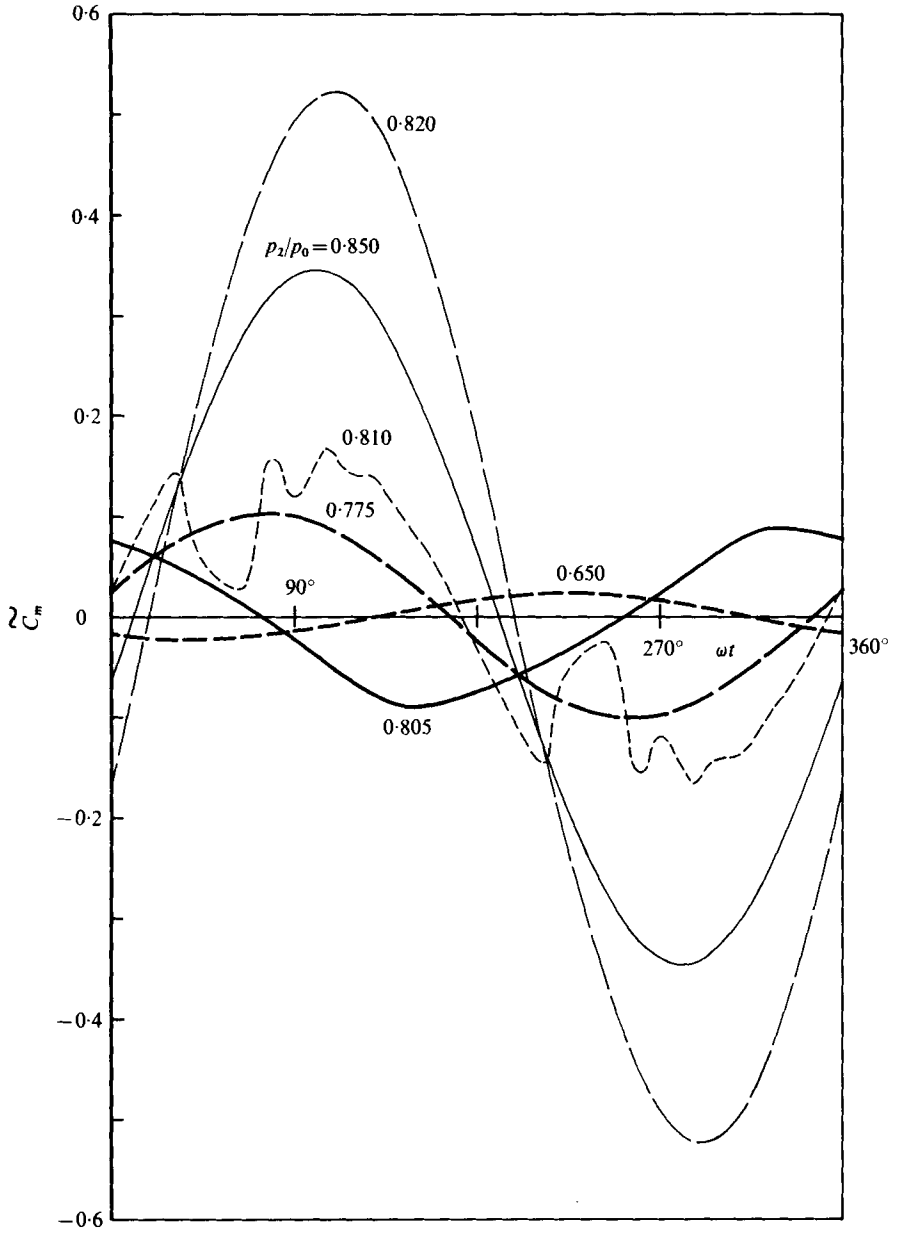

FIGURE 6. Moment *vs.* time. $H/c = 0·5$, $k = 0·092$.

aerodynamic moment. In the subsonic region as well as deep in the transonic region, the unsteady aerodynamic moment varies in an almost sinusoidal manner, whereas in the incipient transonic region the variation is highly distorted. By referring to figure 5, this distortion of the aerodynamic moment can be attributed to an alternation between two distinct states, which depend on whether or not the shocks exist on both sides of the aerofoil.

Figure 7(*a*) compares the fundamental component of the complex aerodynamic moment, obtained from the moment–time history of figure 6, with the experimental

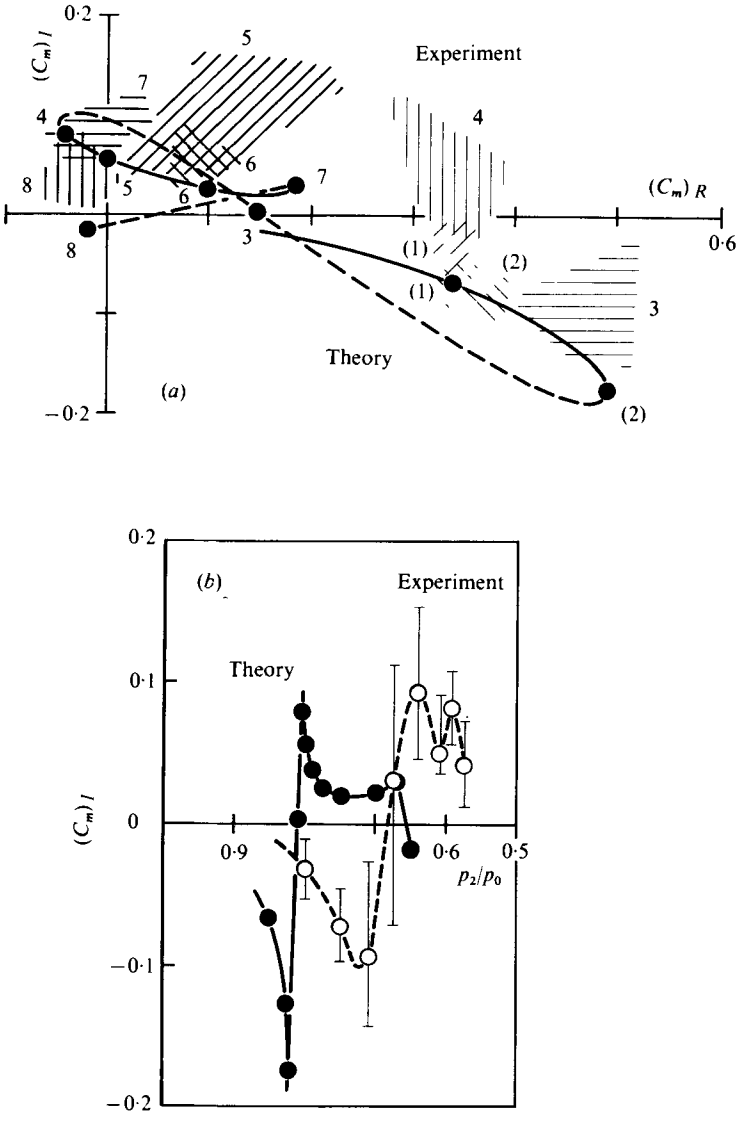

FIGURE 7. Comparison of calculation and experiment. $H/c = 0{\cdot}5$, $k = 0{\cdot}092$. (*a*) Moment coefficient. (*b*) Aerodynamic damping.

(*a*)

Experiment p_2/p_0		Theory p_2/p_0	
(1)	0·800	(1)	0·850
(2)	0·750	(2)	0·820
3	0·710	3	0·810
4	0·676	4	0·805
5	0·642	5	0·800
6	0·610	6	0·775
7	0·594	7	0·670
8	0·577	8	0·650

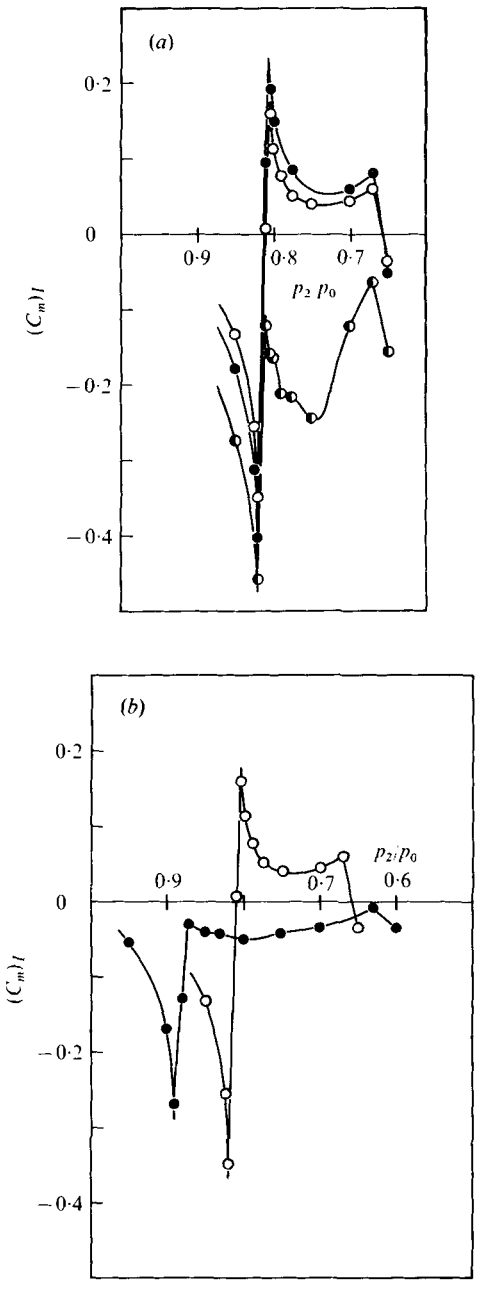

FIGURE 8. Variation of aerodynamic damping due to (*a*) frequency of oscillation and (*b*) channel height. $\bar{\theta} = 0{\cdot}5°$. (*a*) $H/c = 0{\cdot}5$; ○, $k = 0{\cdot}092$; ●, $k = 0{\cdot}139$; ◐, $k = 0{\cdot}462$. (*b*) $k = 0{\cdot}092$; ●, $H/c = 0{\cdot}3$; ○, $H/c = 0{\cdot}5$.

results given in figure 3(*b*, iv). Figure 7(*b*) gives the measured and calculated characteristics of aerodynamic damping, which is defined as $-(C_m)_I$. For the test results not only the averaged values but also the ranges of scatter are shown. The numerical results predict that in the incipient transonic region a slight change in the back-pressure ratio

induces variation of the aerodynamic moment in a marked and discontinuous manner, which leads to negative aerodynamic damping, i.e. system instability, in the transonic region. The discontinuity in the moment may be closely related to the appearance of the shocks, which are very sensitive to the back-pressure variation in the incipient transonic region and bring about a discontinuous change in the pressure distribution around the aerofoil.

As may be seen from figure 7, a comparison of the calculated and experimental results shows good qualitative agreement in all regions, but with a discrepancy in the back-pressure ratio. This appears to give substance to the previous speculation that the scatter of the experimental data in the incipient transonic region may follow the back-pressure variations.

Further calculations were carried out in order to examine the effects of the amplitude and frequency of oscillation and of the channel height. It was found that the aerodynamic damping is only slightly affected by the oscillation amplitude in the range $\bar{\theta} = 0{\cdot}25°$–$1{\cdot}0°$, so that calculated results are presented only for the other factors in figure 8. Figure 8 (*a*) shows that in the lower frequency range $|(C_m)_I|$ increases with increasing oscillation frequency in both the subsonic and the transonic region, but that at much higher frequencies the aerodynamic damping would be positive (i.e. $(C_m)_I$ would be negative) even in the transonic region. The critical back-pressure ratio at which the aerodynamic damping vanishes is nearly constant irrespective of both the amplitude and the frequency of oscillation. Figure 8 (*b*) illustrates the effect of channel height. For a small channel height, such as $H/c = 0{\cdot}3$, the aerodynamic damping characteristics becomes significantly different from the case $H/c = 0{\cdot}5$. For $H/c = 0{\cdot}3$, the aerodynamic damping remains positive in both the subsonic and the transonic region, although a discontinuity still exists between them.

Finally, it may be noted that at a moderate channel height the system considered becomes unstable (i.e. choking flutter may occur) when the aerofoil passages are choked, but becomes stable again for smaller channel heights.

5. Concluding remarks

This paper has considered the aeroelasticity of an aerofoil oscillating in pitch about the midchord in transonic compressible flow between parallel walls. The experiment described indicates that in the transonic regime, where the aerofoil passages are choked, the aerodynamic features are distinct from those in the subsonic regime, and that a discontinuous change occurs in the incipient transonic regime. The problem was also examined through one-dimensional analysis for small channel heights. A comparison of the calculated results with the experimental ones shows good qualitative agreement, supporting the experimental findings. Thus the results obtained demonstrate the possibility of choking flutter in transonic channel flow.

It should be noted that, even for a very small oscillatory angle of attack, the variations in moment are not necessarily small nor sinusoidal, so that the linear superposition may not be always applicable to the present flow. Furthermore, the time-dependent behaviour of the shocks may be very sensitive to the aerofoil profile, so that the conclusions from results obtained should be restricted to the particular case examined. For much smaller channel heights such as $H/c \leqslant 0{\cdot}3$, shock/boundary-layer interactions would produce the so-called pseudo-shock, which would introduce further

complexity and probably make the theoretical assumption of a normal shock inappropriate.

Appendix. Derivation and solution of characteristic equations

Consider one-dimensional continuous flow in a passage whose area A is a function of both time t and position x (see figure 4). The fluid is assumed to be a thermally non-conducting perfect gas. The general forms of the continuity and momentum equations are, respectively,

$$\frac{\partial}{\partial t}(\rho A)+\frac{\partial}{\partial x}(\rho u A)=0, \quad \frac{\partial u}{\partial t}+u\frac{\partial u}{\partial x}+\frac{1}{\rho}\frac{\partial p}{\partial x}=0,$$

where u, p and ρ denote the flow velocity, the pressure and the fluid density. Applying the equation of state and the expressions for the velocity of sound a and entropy s to the above equations gives the characteristic equations in their final forms:

$$\left(\frac{\partial \xi}{\partial t}\right)_+ = -a\frac{D}{Dt}(\log A)+\frac{a}{\gamma R}\left(\frac{\partial s}{\partial t}\right)_+ +\frac{a}{C_p}\frac{Ds}{Dt},$$

$$\left(\frac{\partial \eta}{\partial t}\right)_- = -a\frac{D}{Dt}(\log A)+\frac{a}{\gamma R}\left(\frac{\partial s}{\partial t}\right)_- +\frac{a}{C_p}\frac{Ds}{Dt},$$

where

$$\xi=\frac{2}{\gamma-1}a+u, \quad \eta=\frac{2}{\gamma-1}a-u, \quad \frac{D}{Dt}=\frac{\partial}{\partial t}+u\frac{\partial}{\partial x}, \quad \left(\frac{\partial}{\partial t}\right)_\pm=\frac{\partial}{\partial t}+(u\pm a)\frac{\partial}{\partial x}$$

and γ, R and C_p are the ratio of specific heats, the gas constant and the specific heat at constant pressure, respectively. Entropy is conserved for any fluid mass, so that the following energy equation holds:

$$Ds/Dt=0.$$

In order to simplify the problem, the following matching conditions are used in the present paper. First, the inlet stagnation temperature and entropy are held constant:

$$\tfrac{1}{2}u^2+\frac{1}{\gamma-1}a^2=\frac{1}{\gamma-1}a_0^2, \quad s=s_0 \quad \text{at} \quad x=0.$$

Second, the exit condition is that at the trailing edge the static pressure should be constant and equal to the back-pressure: $p=p_2$ at $x=c$. Finally, when the passage is choked a normal shock is assumed to appear aft of the throat, for which the quasi-steady forms of the Rankine–Hugoniot relation and the energy conservation relation hold:

$$s_4-s_3=C_p\log\left\{\frac{(\gamma+1)p_3+(\gamma-1)p_4}{(\gamma-1)p_3+(\gamma+1)p_4}\left(\frac{p_4}{p_3}\right)^{1/\gamma}\right\},$$

$$\tfrac{1}{2}(u_3-v)^2+\frac{1}{\gamma-1}a_3^2=\tfrac{1}{2}(u_4-v)^2+\frac{1}{\gamma-1}a_4^2,$$

where the subscripts 3 and 4 denote the states just upstream and downstream of the shock respectively and v is the velocity of the moving shock.

The flow velocity, the velocity of sound and the pressure are given respectively by

$$u = \tfrac{1}{2}(\xi - \eta), \quad a = \tfrac{1}{4}(\gamma - 1)(\xi + \eta), \quad \frac{p}{p_0} = \left(\frac{a}{a_0}\right)^{2\gamma/(\gamma-1)} \exp\left(-\frac{s - s_0}{R}\right).$$

The above equations were solved numerically by a finite-difference method. In the present calculations, the aerofoil passage was divided into fifty equal steps, i.e. $\Delta x = \frac{1}{50}c$, and the time step Δt was chosen to be not larger than the maximum value of $\Delta x/(u+a)$.

REFERENCES

CARTER, D. S. & KILPATRICK, D. A. 1957 Self-excited vibration of axial-flow compressor blades. *Proc. Inst. Mech. Engrs* **171**, 245–281.

HAMMITT, A. G. 1975 Unsteady aerodynamics of vehicles in tubes. *A.I.A.A. J.* **13**, 497–503.

MIKOLAJCZAK, A. A., ARNOLDI, R. A., SNYDER, L. E. & STARGARDTER, H. 1975 Advances in fan and compressor blade flutter analysis and predictions. *J. Aircraft* **12**, 325–332.

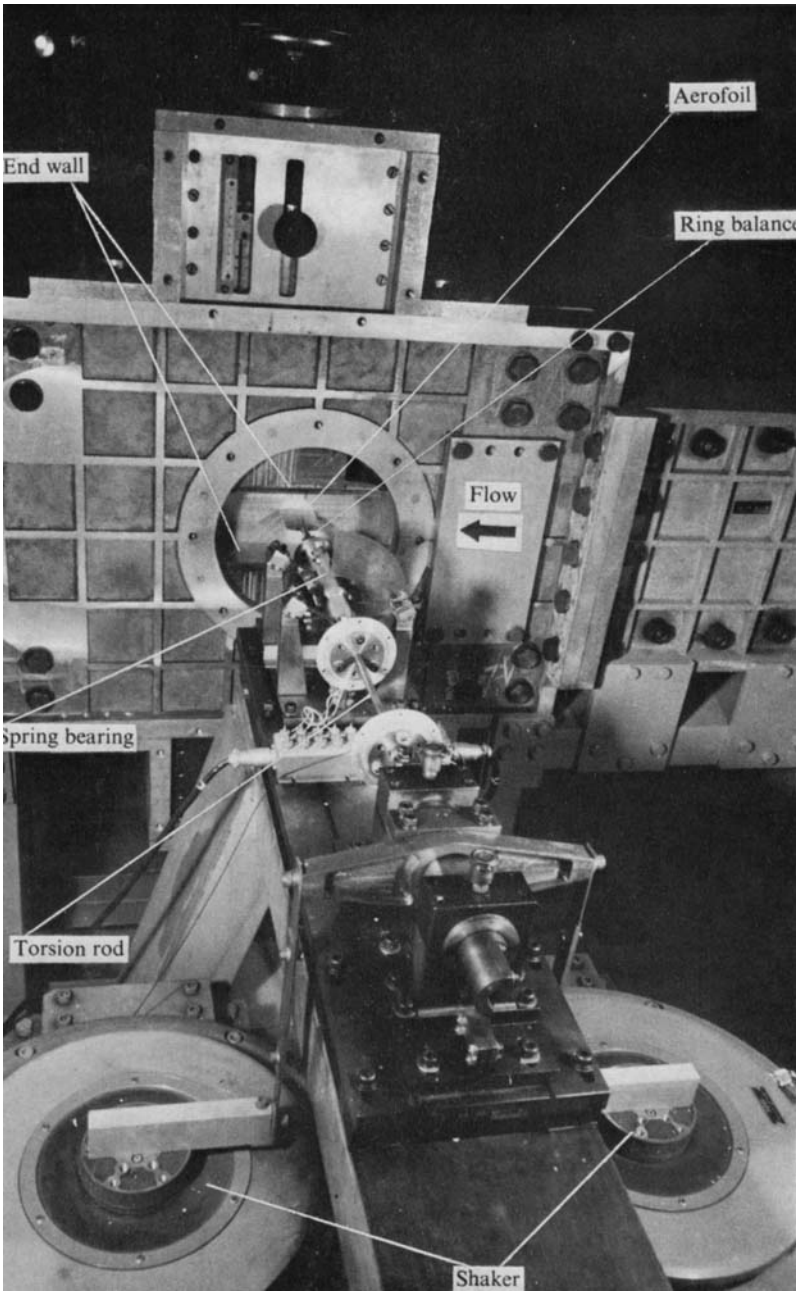

FIGURE 2. Experimental apparatus: test section and pitch oscillation mechanism.